Online Supplementary Appendix for:

Mechanisms of response and resistance to combined decitabine and ipilimumab for advanced myeloid disease

Supplementary methods

Amplicon sequencing

Sequencing of recurrent somatic mutations was performed on DNA extracted from bone marrow aspirates using a targeted multiplex PCR approach by the hematopathology division at Brigham and Women's hospital as previously described.[1]

Bulk RNA-seq gene pattern changes across time points

To explore the effect of Decitabine treatment, we combined DESeq2[2] results that used Screening time point samples versus post-decitabine time point samples (Lead-in, C1, C4). The significant common genes were identified from Screening vs Lead-in, Screening vs C1 and Screening vs C4. The differentially expressed gene list (**Suppl. Fig. 6A**) was generated by overlapping the significant common genes from all three comparisons, but only using paired samples to reduce the effects of tumor heterogeneity.

Bulk RNA-seq immune cell estimation

The selection of which RNA bulk immune cell estimation results to use were based on the correlation with single cell immune cell estimates. For myeloid cells, **Suppl. Table 4** summarizes which cells were combined from each bulk RNA-seq tool to represent the category called "myeloid cells". The single cell RNA-seq immune cell estimates from the following categories were included to estimate "myeloid cell" quantities: HSC, LMPP, GMP, CD14 Mono, CD16 Mono, pDC, cDC2, Prog_DC.

Quantiseq[3] was chosen to represent the infiltrating immune cell component in the bulk RNA-seq samples since it had the highest correlation to the single-cell data.

Whole exome sequencing – DNA and germline controls

WES was performed on DNA extracted from bone marrow aspirates using the QIAamp DNA Blood Midi Kit (Qiagen, Cat. no. 51185). Donor-derived germline DNA was kindly provided by Jonathan Stevens from the Tissue Typing Laboratory at Brigham and Women's hospital. Recipient-derived germline DNA was obtained either through DNA extraction from T cells after 14 days of in-vitro expansion in RPMI supplemented with 10 % FBS, 500 IU/ml IL-2 and 1 % Phytohaemagglutinin P (PHA [only in the first 24 hours]) or DNA extraction from in-vitro culture of bone marrow-derived fibroblasts in DMEM supplemented with 20% FBS, 1% sodium pyruvate (Corning, Cat. no. 25-000-CI), 1% nonessential amino acids (Corning, Cat. no. 25-025-CI), 1% HEPES buffer (Corning, Cat. no. 25-060-CI), 1 % penicillin/streptomycin (Life Technologies, Cat. no. 15140122).

Whole exome sequencing – sample selection

Samples from patients who were biopsied both at Screening and C4/EOT were selected from both study arms for a total of 6 timepoint pairs (5 Arm A, 1 Arm B). The Arm A samples met the additional requirement of having both a patient and donor germline sample, while 1 of the 2 Arm B pairs was dropped because the patient matched normal sample failed quality control (<100x coverage).

Single cell RNA sequencing – processing before creation of single cell suspension

Viably frozen bone marrow mononuclear cells (BMMC) were slowly thawed by incubation in a steam bath at 37 degrees celsius. To avoid clotting, BMMC were transferred into prewarmed PBS supplemented with 10 % FBS and 10 % bovine DNase I, grade II (Sigma Aldrich, Cat. no. 10104159001). After centrifugation at 300 g for 5 minutes, cells were rested in RPMI with 10 % DNase I (StemCell Technologies, Cat. no. 07900) for 15 minutes. If >20 % cells were trypan blue, a dead cell removal (Miltenyi Biotec, Cat. no. 130-090-101) was performed. If >0.5 million cells were available, cells were resuspended in 50 µl PBS + 0.04 % BSA (Thermo Fisher, Cat. no. AM2616), incubated with Human TruStainFcX™ (Biolegend, Cat. no. 422302) for 10 minutes and stained with a custom TotalSeq™-C antibody pool for 30 minutes on ice and washed three times.

Single cell RNA sequencing – cell annotation using reference mapping

To ensure consistent cell type annotation across samples and to allow comparison with other single cell datasets, annotations were generated based on a healthy bone marrow dataset. Reference mapping was performed as described in the Seurat documentation using the bmcite dataset.[4]

Single cell RNA sequencing – differential gene expression analyses

Differential gene expression analyses were performed on a per sample and per celltype basis using Seurat::Findmarkers(). Statistically significant changes in gene expression were defined as log2fc > 0.25 and FDR < 10^-10 across 3 independent groups with at least 25 cells per group.

Single cell RNA sequencing – gene module scores

Based on co-incubation experiments of melanoma-infiltrating T cells with autologous tumor cell lines[5] and previous single cell analyses of AML-associated T cells[6], gene module scores were calculated using Seurat::AddModuleScore() based on the expression of *PDCD1, CTLA4, TIGIT, HAVCR2, TOX, LAG3* and *ENTPD1* (exhaustion score) and *TCF7, IL7R, SELL, CCR7, CD28* (memory score).

Single cell RNA sequencing – souporcell

Annotation of donor and recipient-derived cells was performed by deconvolution of samples using *souporcell* on the aligned bam file produced by cellranger with k=2.[7] The clusters defined by *souporcell* were manually labeled as donor and recipient based on distribution across myeloid and T cell populations as well as known T cell chimerism from routine clinical diagnostics.

Single cell RNA sequencing – CellPhoneDb

Cell-cell interactions were discovered using *CellPhoneDB*[8] based on its curated database and quantified per cell type, individual and timepoint.

Single cell RNA sequencing – T cell receptor analysis

T cell clones were defined based on CDR3β amino acid sequences using a custom script. Statistically significant changes in T cell clone abundance were detected using a Fisher exact test and FDR correction with a cut-off of $p < 0.0001$.

Clonal T cell expansion was defined as the percentage of T cells that share the same T cell receptor amongst all identified T cell clones of the same sample.

Single cell RNA sequencing data – CML dataset

3' single cell gene expression profiles of CML[9] were reanalyzed starting from raw sequencing reads with the same analytical steps as AML samples. They are deposited on dbGap (phs001998.v3).

Bulk RNA sequencing analysis of bone marrow and extramedullary AML

A count matrix from processed bulk RNA-seq gene expression data was obtained from FFPE biopsies as transcripts per million reads (TPM) as previously described.[10] TPM values were analyzed using custom scripts in Rstudio and visualized with ggplot2.

Multiplexed immunofluorescence staining

Staining was performed on the BOND RX fully automated stainers (Leica Biosystems). Tissue sections of 5-µm thick FFPE were baked for 3 hours at 60°C before loading into the BOND RX. Slides were deparaffinized (BOND DeWax Solution, Leica Biosystems, Cat. AR9590) and rehydrated with series of graded ethanol to deionized water. Antigen retrieval was performed in BOND Epitope Retrieval Solution 1 (pH 6), as shown below (ER1, Leica Biosystems, Cat. AR9961) at 98°C. Deparaffinization, rehydration and antigen retrieval were pre-programmed and executed by the BOND RX. Next, slides were serially stained with primary antibodies with an incubation time of 40 minutes per antibody. As an additional step for mouse antibodies, rabbit anti-mouse IgG (Post Primary, BOND Polymer Refine Detection Kit, Leica Biosystems, Cat. DS9800) was applied for 15 minutes. Signal for antibody complexes was labeled and visualized by their corresponding Opal Fluorophore Reagents (Akoya) by incubating with the slides for 10 minutes. Slides were then manually counterstained with DAPI (NucBlue Fixed Cell ReadyProbes

Reagent, Invitrogen, Cat. R37606), washed with deionized water, air dried, and mounted with ProLong Diamond Anti-fade Mountant (Life Technologies, Cat. P36965). Slides were stored in a light-proof box at 4℃ prior to imaging. The target antigens, antibody clones, dilutions, and antigen retrieval conditions are listed in **Supplementary Table 5**.

Image acquisition was performed using the Mantra Quantitative Pathology Workstation (Akoya Biosciences). Areas with non-tumor or residual normal tissue were excluded from the analysis. Representative regions of interest were chosen under pathologist supervision, and 3-9 fields of view (FOV) were acquired at 20x resolution. Once the FOV were spectrally unmixed, cell identification was performed using supervised machine learning algorithms within Inform 2.4 (Akoya). This image analysis software assigns phenotypes to all cells in the image, based on a combination of immunofluorescence characteristics associated with segmented nuclei (DAPI signal). Each cell-phenotype specific algorithm is based upon an iterative training / test process, whereby a small number of cells (training phase, typically 15-20 cells) are manually selected as being most representative of each phenotype of interest and the algorithm then predicts the phenotype for all remaining cells (testing phase). The software's predictions can be over-ruled to improve accuracy until phenotyping is optimized. Thresholds for "positive" staining and the accuracy of phenotypic algorithms were optimized and confirmed under pathologist supervision.

Supplementary Tables

Suppl. Table 1. Differential gene expression changes between non-responders and responders at screening.
See separate excel file.

Suppl. Table 2. Patient characteristics single cell RNA-seq cohort.

Study ID	Disease Histology	Transplant status	disease state at study entry	%blasts at study entry	Clinical Response on trial	Best objective response category for analysis	Karyotype	Mutated genes
1006	sAML arising from MDS	post-HSCT	relapse	5-10 (core) 11 (aspirate)	CR	Response	46,XX,del(20q)	U2AF1
1007	MDS	post-HSCT	relapse	5-10 (core) 13 (aspirate)	marrow CR without HI	Response	normal	ASXL1, IDH2, RUNX1, SRSF2, STAG2
1019	sAML arising from MDS	post-HSCT	relapse	60 (core) 22 (aspirate)	CR	Response	47,XY,+8[4]/ 47,XY,+21[3]/ 46,XY[8]	ASXL1, RUNX1, STAG2
1010	AML	post-HSCT	relapse	30 (core) 44 (aspirate)	Stable Disease	Non-response	Normal	NRAS, ATM, GATA2, PRPF8
1012	AML	post-HSCT	refractory	50 (core) 32 (aspirate)	Stable Disease	Non-response	complex aberrant with inv(3), del(5q) and add(21)	TP53
1016	tAML	post-HSCT	relapse	30-40 (core)	Stable Disease	Non-response	complex aberrant with del(5q) and del(17p)	none
1022	sAML arising from MDS	post-HSCT	refractory	50 (core) 13 (aspirate)	Stable Disease	Non-response	monosomal complex karyotype	DNMT3A, RUNX1, SF3B1
1026	sAML from MDS/MPN overlap syndrome	post-HSCT	refractory	5 (core) 26 (aspirate)	Stable Disease	Non-response	46,XX,t(9;12)(q22;q13) c[cp20]	ASXL1, GNB1, NRAS, SF3B1, SRSF2
1002	sAML from essential thrombocythemia	transplant-naïve	untreated AML	60 (core) 56 (aspirate)	CR	Response	complex aberrant with del(7q)	IDH2, JAK2, TET2, TP53, U2AF1
1008	sAML arising from MDS	transplant-naïve	untreated AML	30-40 (core) 39 (aspirate)	CR	Response	normal	PHF6, RUNX1, SF3B1, TET2; P2Ry8-CRLF2 fusion
3001	sAML from myelofibrosis	transplant-naïve	untreated AML	20-30 (core) 35 (aspirate)	CRi	Response	normal	ATM, JAK2, NRAS, RUNX1, SRSF2
3003	MDS	transplant-naïve	refractory	17 (core) 14 (aspirate)	marrow CR with HI-P	Response	normal	ASXL1, EZH2, RUNX1, STAG2, TET2, U2AF1, ZRSR2
3005	sAML arising from MDS	transplant-naïve	relapse	5-10 (core) 29 (aspirate)	CR	Response	45,XX, dic(5;17)(q11.2;p11.2)	CUX1, DNMT3A
8002	sAML arising from MDS	transplant-naïve	refractory	12 (aspirate)	CRi	Response	normal	ASXL1, IDH2, SRSF2, STAG2
8007	MDS	transplant-naïve	refractory	10-15 (core) 12 (aspirate)	marrow CR with HI-N, HI-E and HI-P	Response	Monosomal complex karyotype	DNMT3A, TP53
1005	AML	transplant-naïve	refractory	20 (core) 16 (aspirate)	Stable Disease	Non-response	Normal	ASXL1, DNMT3A, IDH1, IDH2
5003	AML	transplant-naïve	relapse	7 (aspirate)	stable disease	Non-response	46,XY,del(7)(q21)[10]/ 47,XY,+8[5]/46,XY[5]	KRAS, RUNX1
8004	sAML arising from CMML	transplant-naïve	refractory	80 (core) 67 (aspirate)	stable disease	Non-response	45,XX,-7[13]/46,XX[7]	PTPN11, SF3B1

Suppl. Table 3. Additional patient characteristics post-HSCT.

Study ID	Best Response	Days post-HSCT	Donor Type	Source	Conditioning Intensity	Conditioning Regimen	IS Plan
1006	CR	151	MUD	PBSC	RIC	FluBu2	MTX/Tac
1007	marrow CR without HI	557	MRD	PBSC	RIC	FluBu2	Siro/Tac
1019	CR	1056	Haplo	BM	RIC	ATG/Cy/Flu/TBI	Tac/MMF
1010	Stable Disease	195	MUD	PBSC	RIC	FluBu2	MTX/Tac
1012	Stable Disease	165	MRD	PBSC	RIC	FluBu2	MTX/Tac
1016	Stable Disease	486	MUD	BM	MAC	FluBu4	MTX/Tac
1022	Stable Disease	367	MUD	PBSC	RIC	FluBu2	MTX/Tac
1026	Stable Disease	299	MUD	PBSC	RIC	FluBu2	MTX/Tac

CR: complete remission, HI: hematologic improvement, MUD: matched unrelated donor, MRD: matched related donor, Haplo: haploidentical donor, PBSC: peripheral blood stem cells, RIC: reduced intensity conditioning, MAC: myeloablative conditioning, Flu: fludarabine, Bu: busulfan, ATG: anti-thymocyte globulin, Cy: cyclophosphamide, TBI: total body irradiation, MTX: methotrexate, Tac: tacrolimus, Siro: sirolimus, MMF: mycophenolate mofetil

Suppl. Table 4. Cell type categories used for identification of myeloid cells using deconvolution tools.

Tool	Cell type
TIMER	Neutrophil
TIMER	Macrophage
TIMER	Myeloid DC
MCPCOUNTER	Monocyte
MCPCOUNTER	Myeloid DC
MCPCOUNTER	Neutrophil
QUANTISEQ	Macrophage
QUANTISEQ	Monocyte
QUANTISEQ	Neutrophil
EPIC	Macrophage
XCELL	Macrophage
XCELL	Neutrophil
XCELL	Myeloid DC
XCELL	Common myeloid progenitor
XCELL	Granulocyte-monocyte
XCELL	Hematopoietic
XCELL	Monocyte
XCELL	Plasmacytoid
CIBERSORT-ABS	Macrophage
CIBERSORT-ABS	Neutrophil
CIBERSORT-ABS	Monocyte
CIBERSORT-ABS	dendritic

Suppl. Table 5. Antibodies used for multiplexed immunofluorescence staining.

Antibody	Clone	Company	Catalog #	Antibody Dilution	Opal Fluor	Fluor Dilution	Antigen Retrieval, Time (min)
Analysis of regulatory T cells							
CD3	Polyclonal	Dako	A0452	1:1000	520	1:100	ER1, 10
FOXP3	206D	BioLegend	320102	1:2000	570	1:150	ER1, 10
Analysis of extramedullary AML and bone marrow							
PD-1	EPR4877(2)	abcam	ab137132	1:500	520	1:75	ER2, 30
CTLA-4	E2V1Z	CST	53560	1:100	540	1:75	ER2, 20
FOXP3	D2W8E	CST	98377	1:200	570	1:225	ER2, 30
CD103	EPR4166(2)	abcam	ab129202	1:150	620	1:125	ER2, 20
CD3	Polyclonal	Dako	A0452	1:600	650	1:200	ER2, 30

Supplementary Figures

Suppl. Fig. 1 Bone marrow analysis.

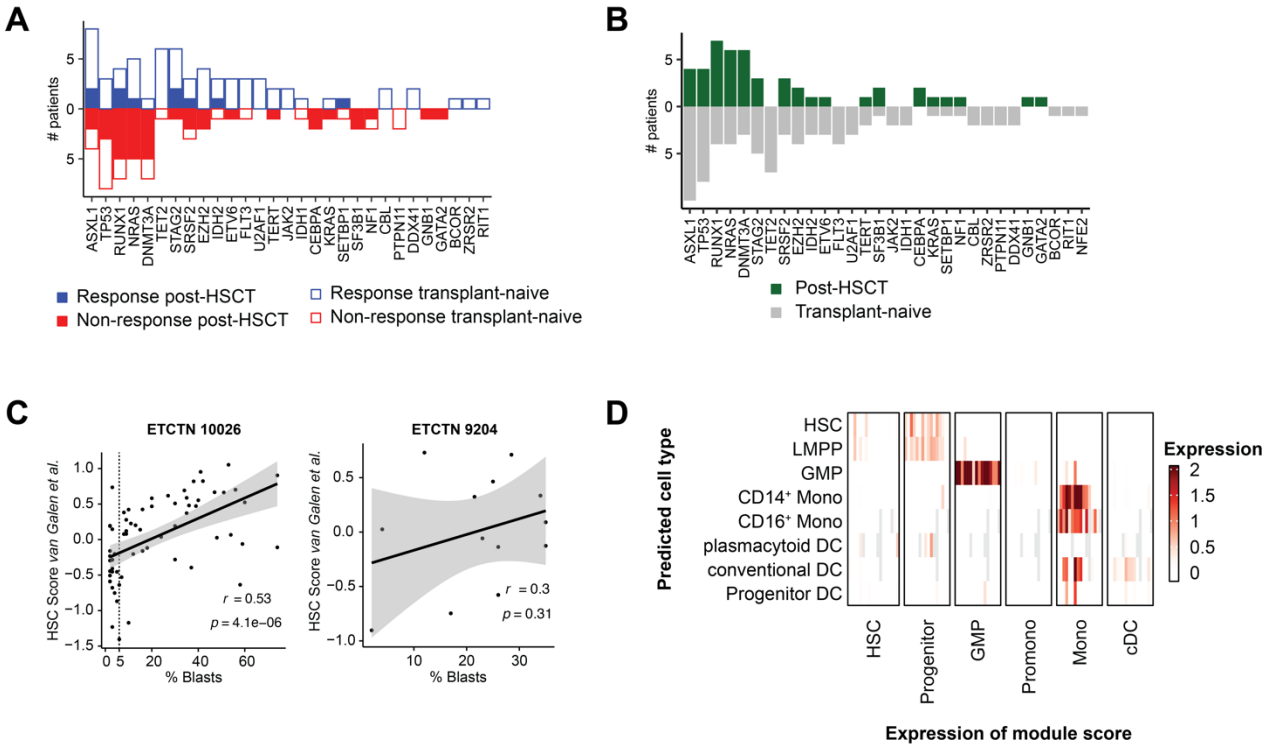

A, B. Distribution of recurrent somatic mutations in patients from ETCTN/CTEP 10026 study grouped by clinical response (A) and study arm (B).
C. HSC score[11] calculated from bulk transcriptomic data obtained in ETCTN/CTEP 10026 and 9204 study correlate with routine clinical data of blast counts (histology and cytology) in bone marrow samples.
D. Expression of gene scores calculated using AML-specific gene sets (HSC, Progenitor, GMP, Promono, Mono, cDC) described in van Galen et al., *Cell* 2019[11] across predicted cell types.

Suppl. Fig. 2. Detectable copy number changes in myeloid cell subsets.

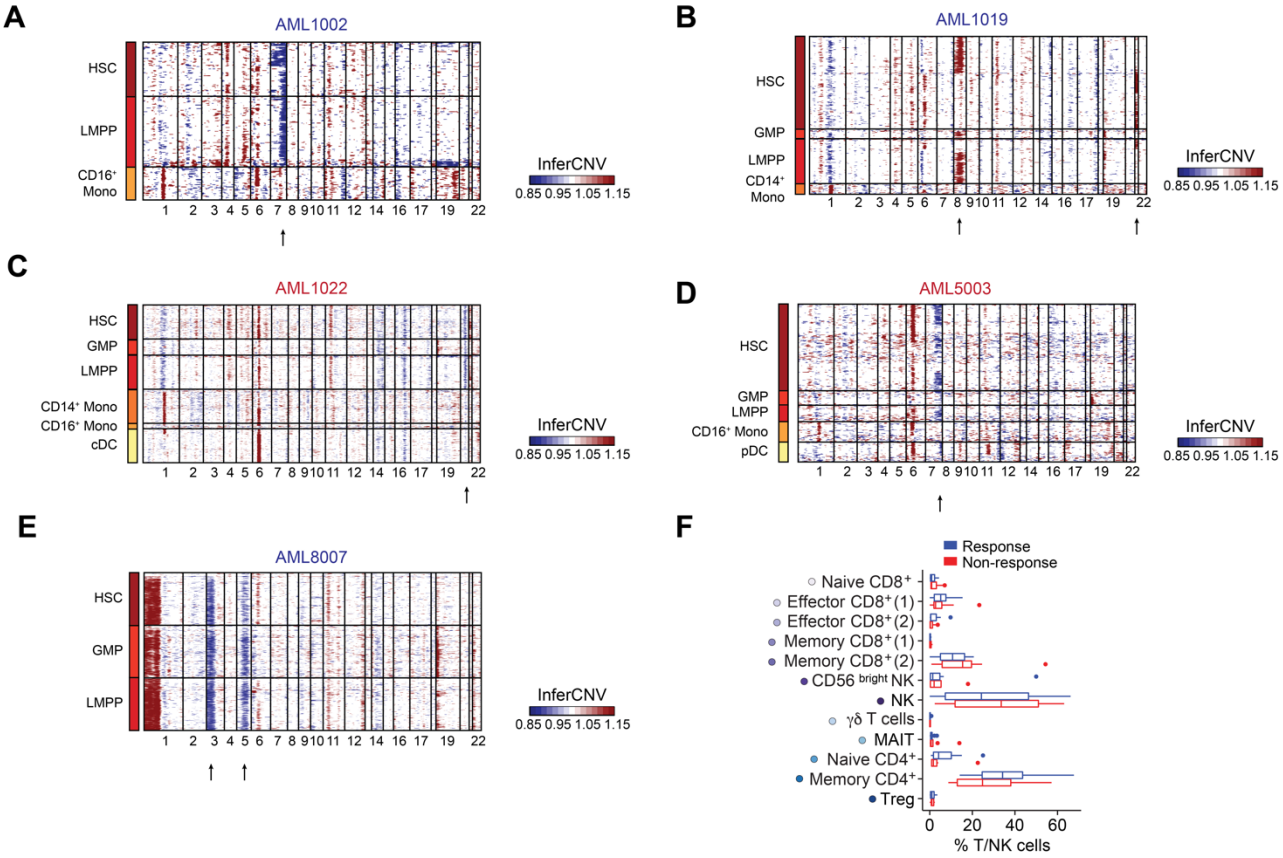

A-E. Copy number changes calculated using *inferCNV* across myeloid cell types in 5 screening samples. AML1002, AML1019, AML8007 – responders. AML1022, AML5003 – non-responders. Arrows indicate known copy number changes from clinical karyotyping.

F. Abundance of T/NK cell subsets in responders (n=10) and non-responders (n=8) at screening does not provide prediction of clinical response during decitabine and ipilimumab treatment.

Suppl. Fig. 3 Bulk sequencing cell type estimation and bulk plasma analyte analysis.

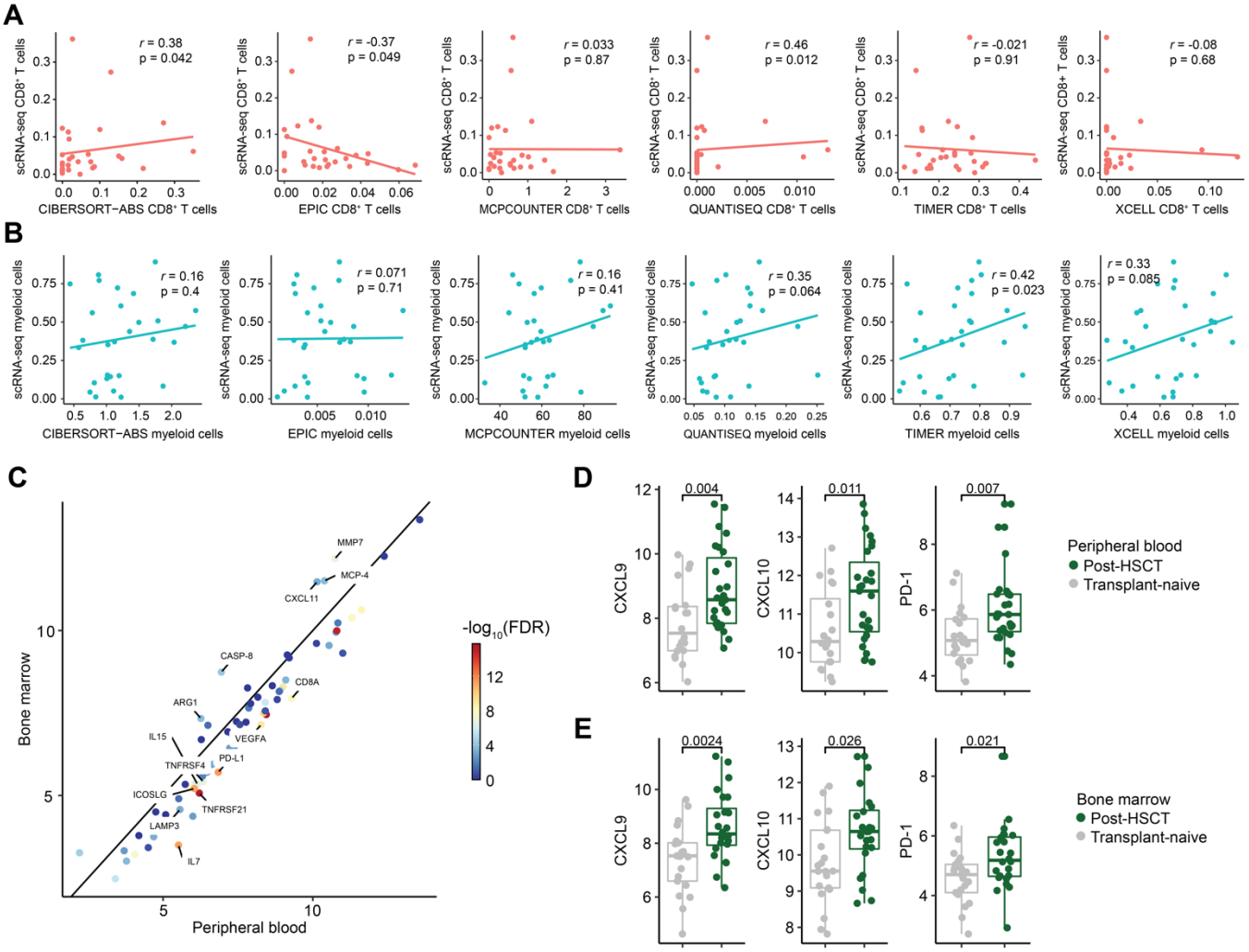

A-B. Correlation of cell type estimation using single cell sequencing and different deconvolution methods for bulk transcriptomic data.

C. High correlation of plasma expression profiles between bone marrow and peripheral blood. Statistically significant differences are labeled. Colors indicate FDR corrected level of significance.

D-E. Post-transplant samples have higher expression of CXCL9, CXCL10 and PD-1 in peripheral blood (D) and bone marrow (E). Statistical testing using Student's t-test.

Suppl. Fig. 4. Correlation of response-associated cytokines with disease burden.

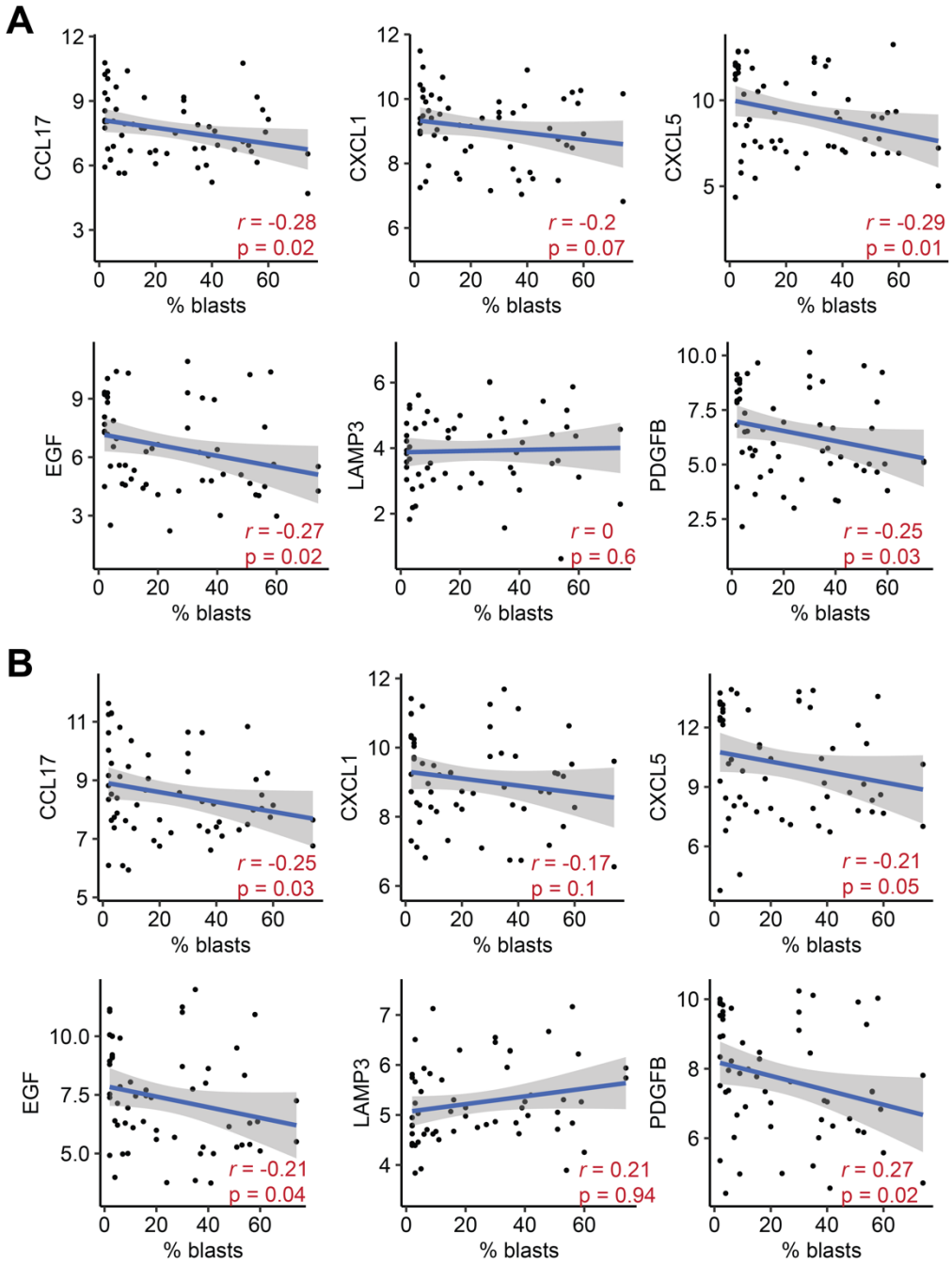

A-B. Correlation of circulating blast counts with expression of cytokines in bone marrow (A) and peripheral blood (B). Blue lines indicate lines of best fit. Grey areas indicate the 95% confidence interval. Correlation coefficients and p values calculated using Pearson's product-moment correlation.

Suppl. Fig. 5. Pharmacodynamics of decitabine.

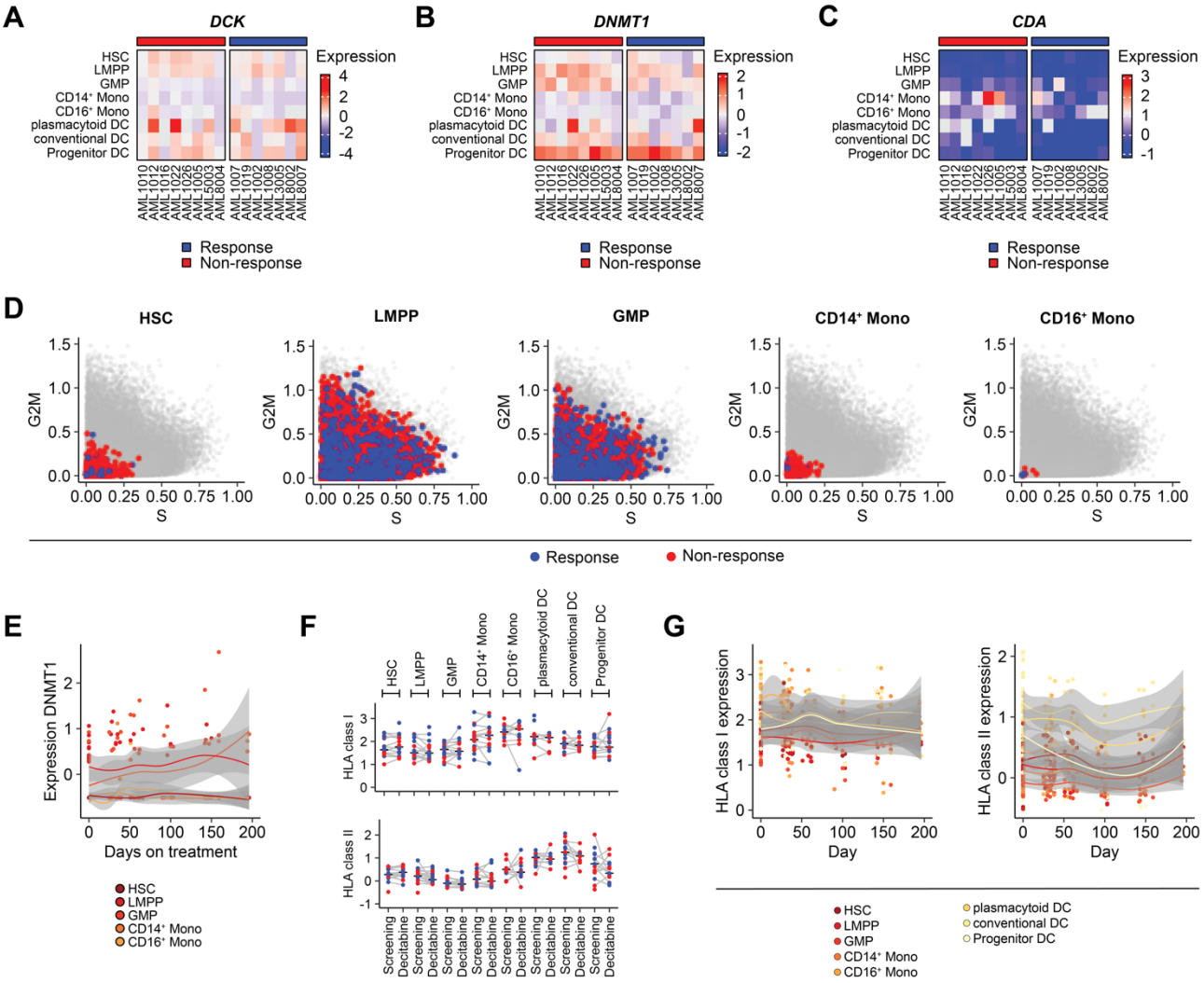

A-C. Expression of *DCK*, *DNMT1* and *CDA* across myeloid cell subsets for individual AML samples.
D. S and G2/M gene score of different myeloid cell subsets.
E. Longitudinal expression of *DNMT1* across myeloid cell subsets.
F, G. Expression of HLA class I and HLA class II genes across myeloid cell subsets at study entry (Screening) and after one cycle of decitabine (Decitabine) (F) and over time (G).

Suppl. Fig. 6. Pharmacodynamics of decitabine and ipilimumab.

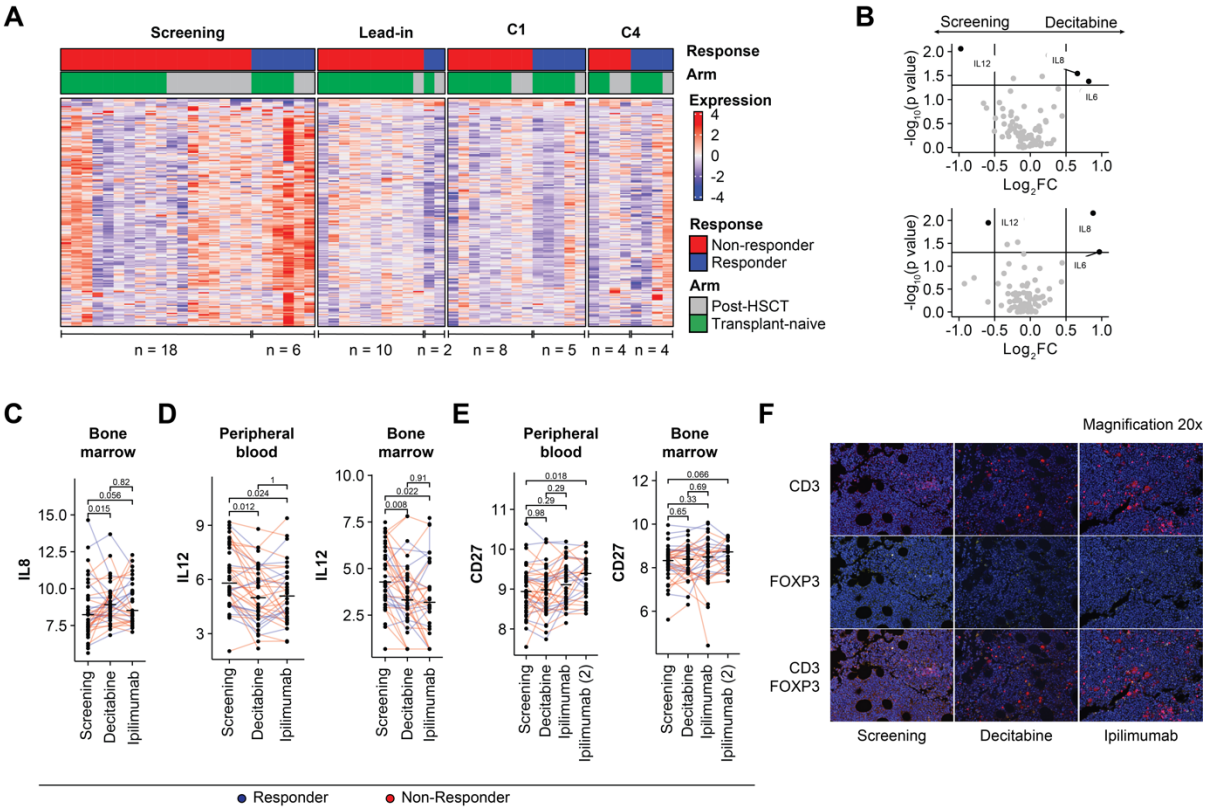

A. Differentially expressed genes in bulk RNA sequencing data from bone marrow core biopsies at screening, after 1 cycle of decitabine (Lead-in), after 2 cycles of decitabine and 1 cycle of ipilimumab (C1) and at a later timepoint (C4).
B. Differential expression of plasma proteins before and after treatment with decitabine in peripheral blood (top) and bone marrow (bottom).
C-E. Plasma levels of soluble IL-8, IL-12 and CD27 in peripheral blood and bone marrow throughout treatment with decitabine and ipilimumab. Blue – responders, red – non-responders.
F. Staining of CD3 and FOXP3 in bone marrow of one patient at study entry (Screening), following one cycle with decitabine (Decitabine) and after addition of ipilimumab (Ipilimumab).

Suppl. Fig. 7. Marker gene expression on T cell subpopulations.

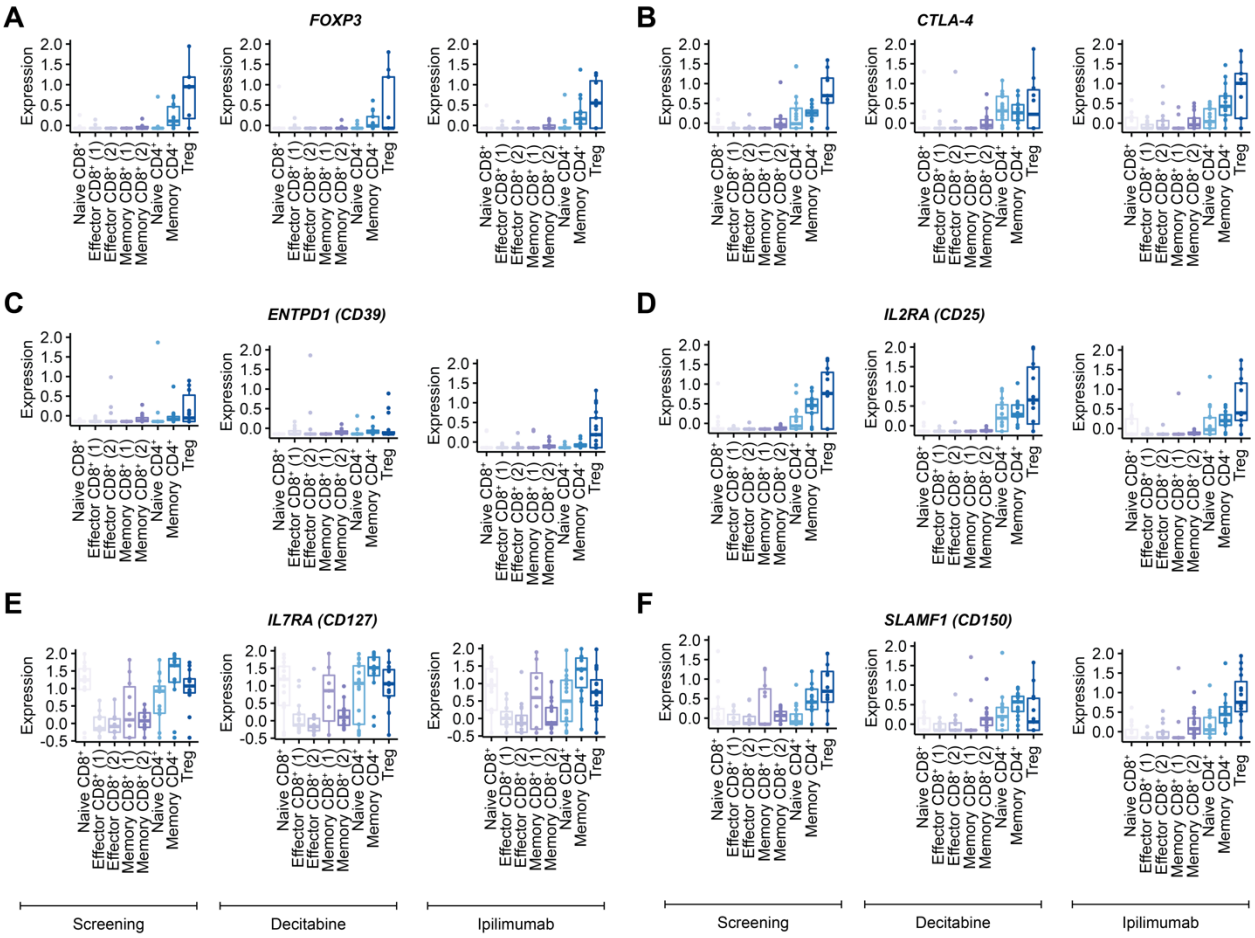

A-F Single cell gene expression of *FOXP3*, *CTLA-4*, *ENTPD1* (encoding CD39), *IL2RA* (CD25), *IL7RA* (CD127), *SLAMF1* (CD150) on T cell subpopulations shown for 18 patients at study entry (Screening), following decitabine priming (Decitabine) and following combined decitabine and ipilimumab treatment (Ipilimumab).

Suppl. Fig. 8. Longitudinal tracking of recurrent somatic mutations throughout the study in responders and non-responders.

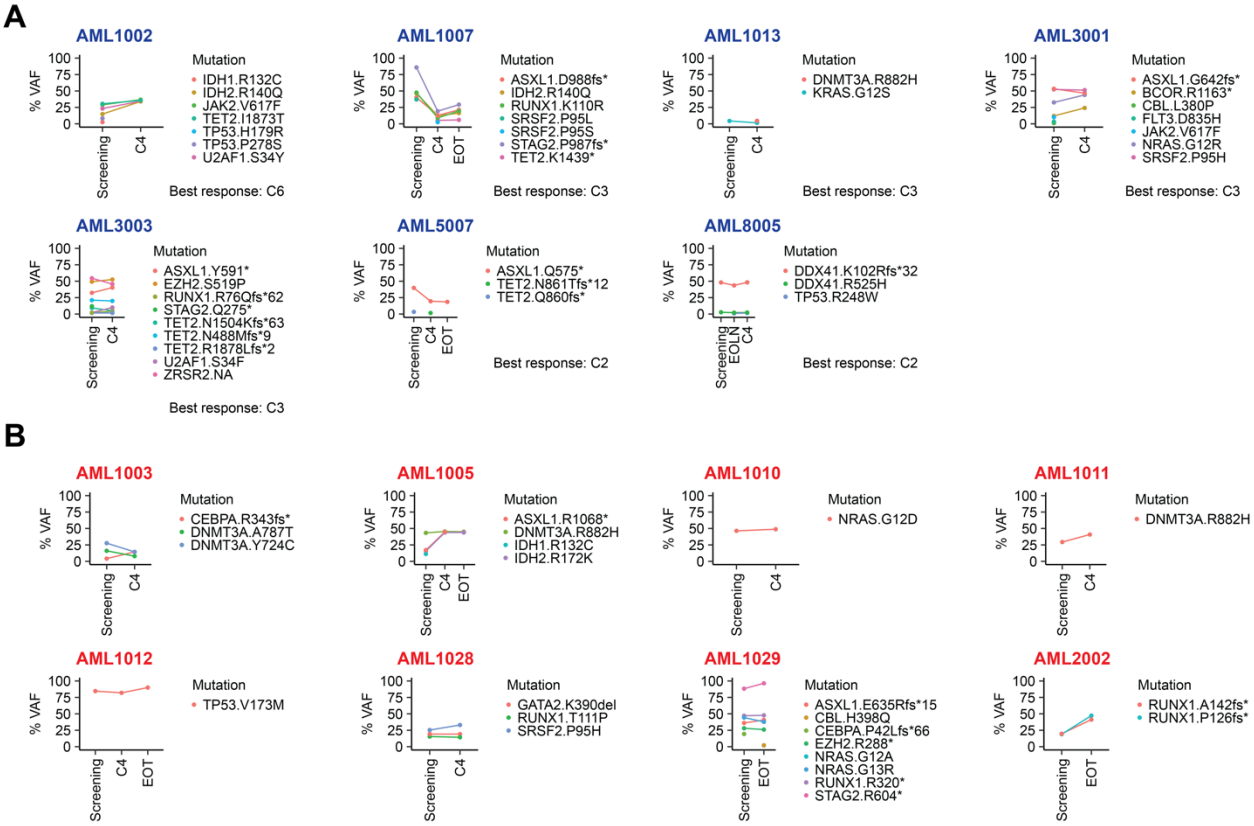

A, B. Longitudinal variant allele frequencies of somatic mutations obtained through targeted sequencing from bone marrow aspirates at study entry (Screening), after 4 cycles of combined decitabine and ipilimumab (C4) and at the end of treatment (EOT). Responders are shown in blue (A) and non-responders in red (B). Time of best response for AML responders is indicated.

Suppl. Fig. 9. Longitudinal stability of genetic changes in AML.

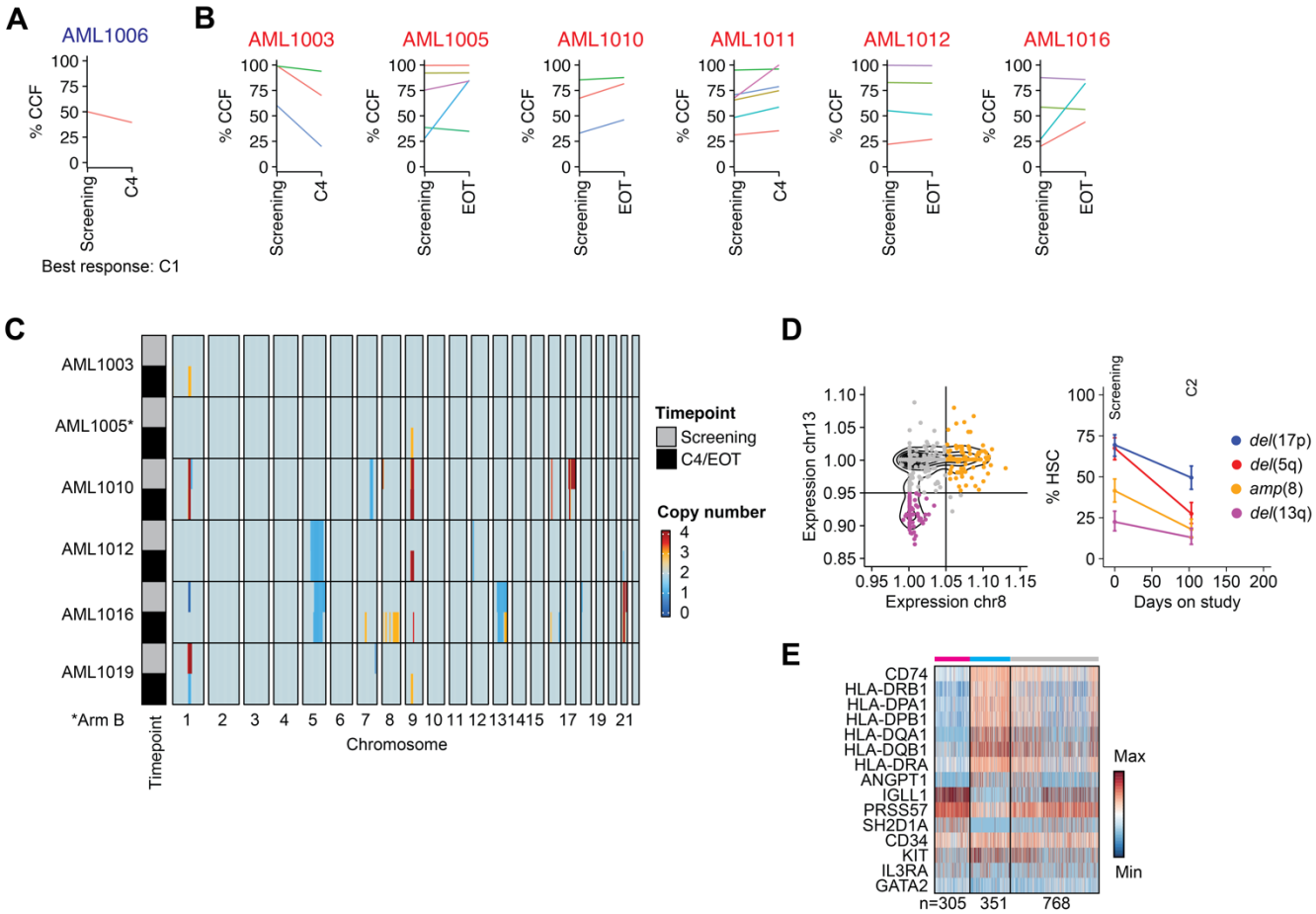

A, B. Cancer cell fraction (CCF) calculated from whole exome sequencing (WES) data of bone marrow aspirates at screening, after 4 cycles of decitabine and ipilimumab or at end of treatment (EOT) for responders (A) and non-responders (B).

C. Copy number changes calculated from WES data at study entry (Screening) and at a later timepoint (C4 or EOT).

D. Stability of copy number changes calculated using *inferCNV* for AML1016.

E. Differential gene expression across clone 1 (pink) and clone 2 (cyan) of HSC cluster in AML1019. Grey – cells not annotated to either clone.

Suppl. Fig. 10. Expression of T cell genes associated with T cell exhaustion.

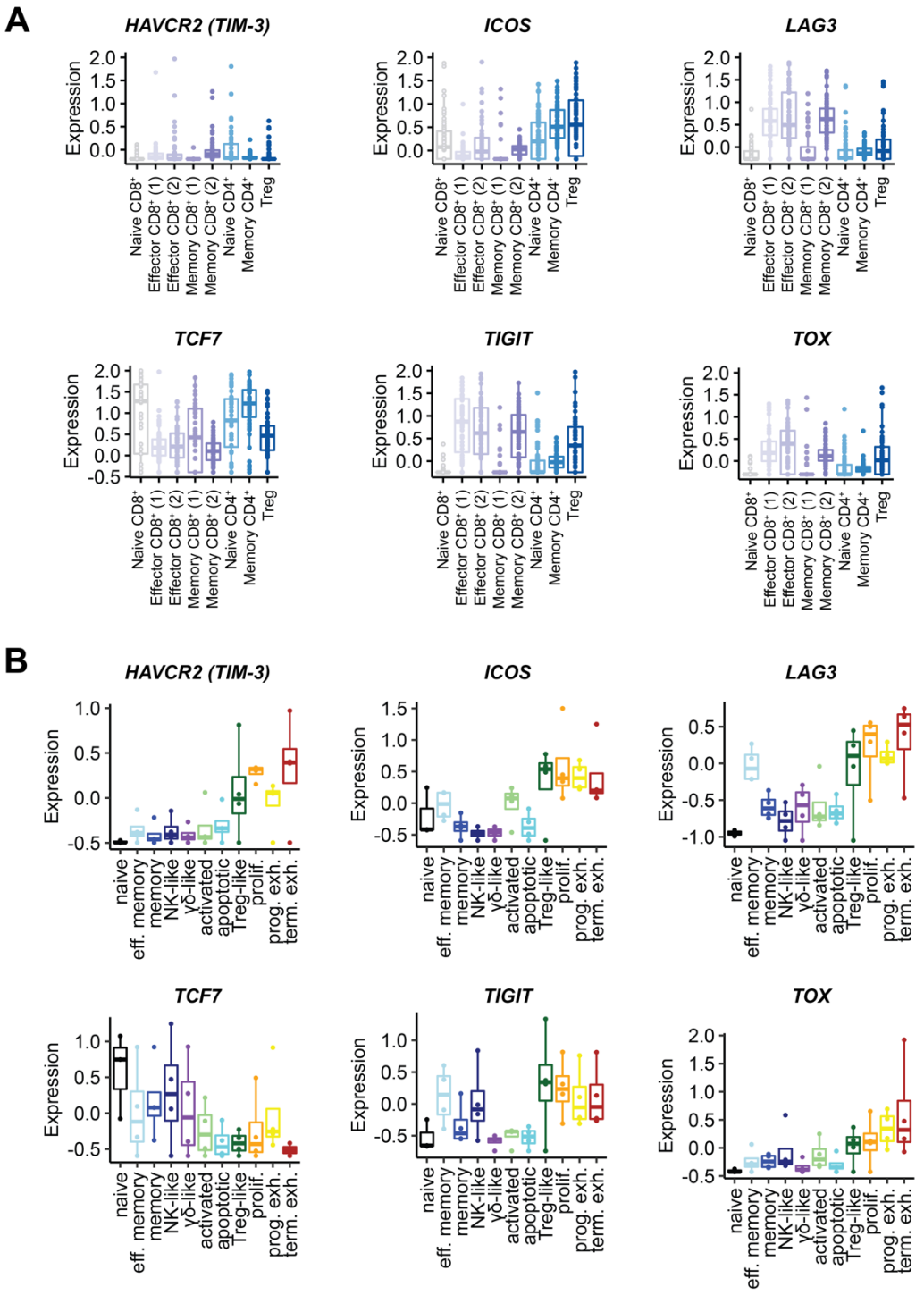

A, B. Single cell expression data shown for AML bone marrow-associated T cell subsets (A) and melanoma-infiltrating $CD8^+$ T cells from Oliveira et al., *Nature* 2021[5] (B).

Suppl. Fig. 11. T cell exhaustion in CD4$^+$ T cells associated with bone marrow and solid tumors.

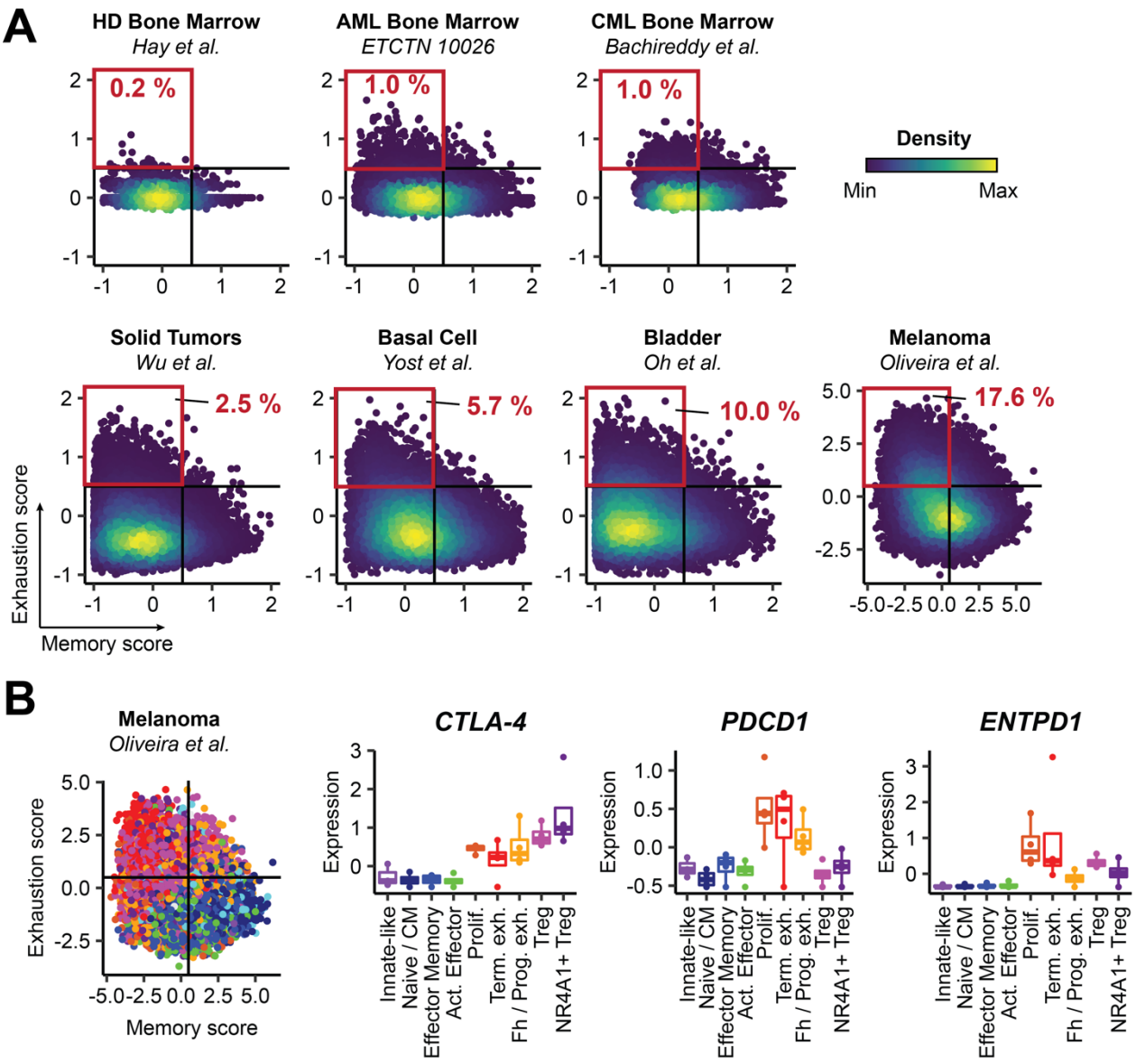

A. T cell exhaustion and memory scores calculated for CD4$^+$ T cells from healthy bone marrow[12], AML and CML[9] bone marrow and different solid tumors[13] including basal cell carcinoma[14], bladder cancer[15] and metastatic melanoma[16].

B. Exhaustion and memory score in CD4$^+$ T cells from metastatic melanoma color by subset (left). Gene expression of *CTLA-4*, *PDCD1* (encoding PD-1) and *ENTPD1* (CD39) shown for CD4$^+$ T cell subsets (right).

Suppl. Fig. 12. T cell phenotypes in AML and CML.

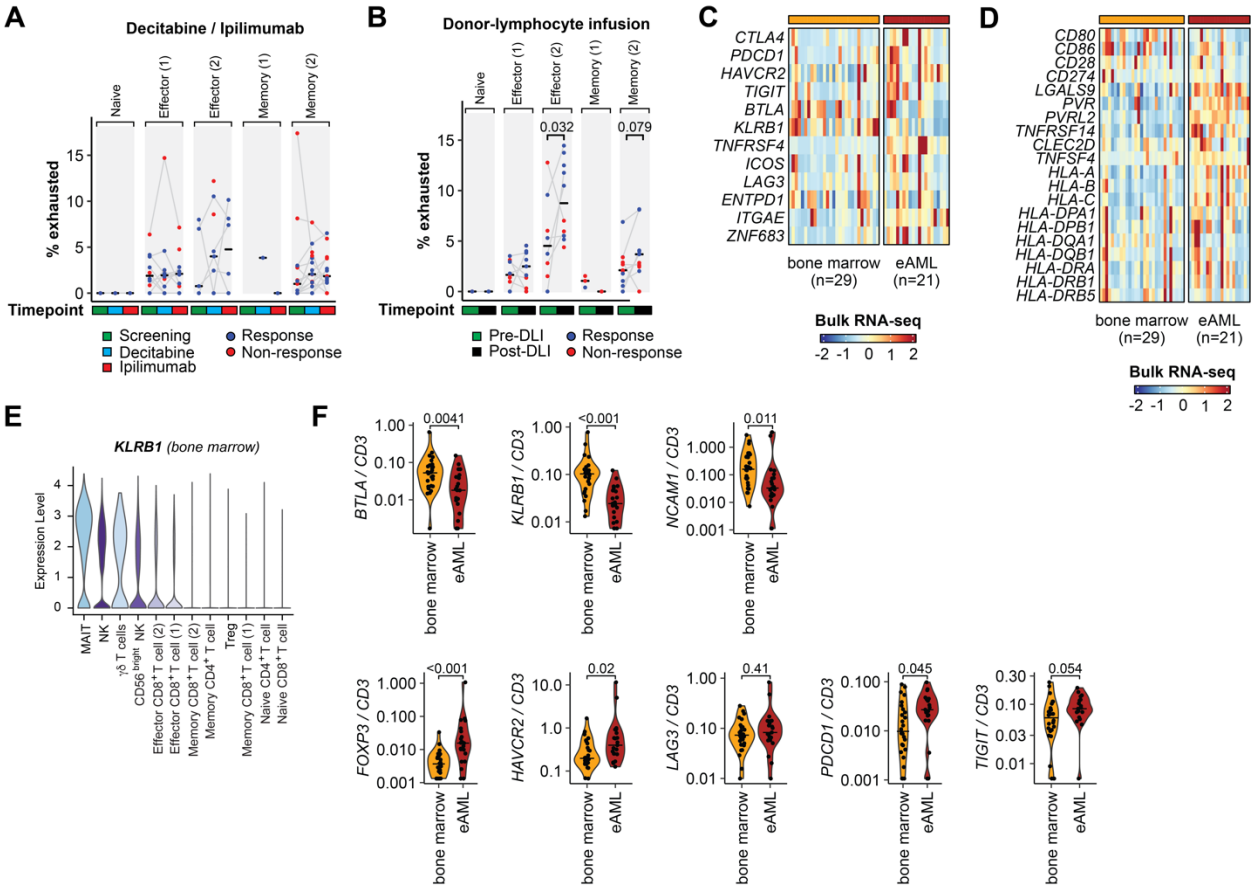

A-B. Stability of percentage of T cells with high exhaustion score in AML following decitabine and ipilimumab treatment shown together for transplant-naïve and post-transplant context (A). Increase in percentage of effector $CD8^+$ T cells with high exhaustion score of in CML following donor-lymphocyte infusion (DLI) (B).
C-D. Expression of T cell-associated genes in bulk RNA sequencing data of AML/MDS bone marrow (n=29) and extramedullary AML (eAML, n=21) biopsies obtained during ETCTN/CTEP 9204 study[10].
E. *KLRB1* expression obtained from single cell RNA profiles of AML bone marrow across T and NK subpopulations.
F. Ratio of T cell marker and immune checkpoint molecule genes relative to CD3 gene expression in bulk RNA sequencing data of bone marrow and eAML.

Suppl. Fig. 13. T cell phenotypes in bone marrow AML and leukemia cutis.

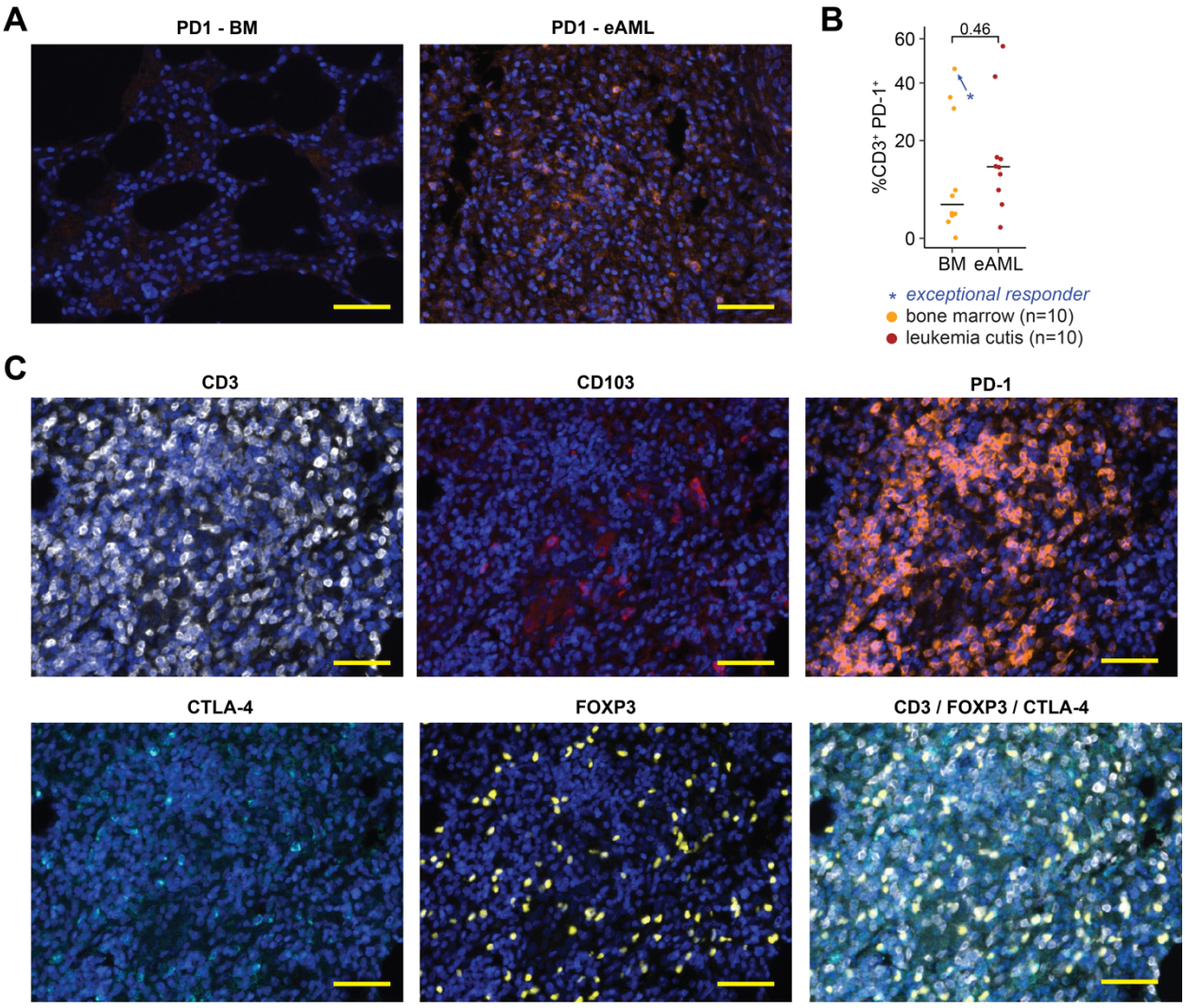

A. Representative stains of PD1 in bone marrow (BM) and leukemia cutis (eAML). The yellow bars indicate a distance of 50 µm.
B. PD-1 expression on T cells in bone marrow and leukemia cutis. Statistical testing with two-sided student's t-test. Medians are indicated for each group by the horizontal bar.
C. Expression of CD3, CD103, PD-1, CTLA-4, FOXP3 and CD3/FOXP3/CTLA-4 in bone marrow of exceptional responder 1006 before treatment with decitabine and ipilimumab. The yellow bars indicate a distance of 50 µm.

The images were captured with 20x optical magnification and 250% zoom.

Supplementary references

1. Kluk MJ, Lindsley RC, Aster JC, et al. Validation and Implementation of a Custom Next-Generation Sequencing Clinical Assay for Hematologic Malignancies. *J Mol Diagn*. 2016;18(4):507–515.
2. Love MI, Huber W, Anders S. Moderated estimation of fold change and dispersion for RNA-seq data with DESeq2. *Genome Biology*. 2014;15(12):550.
3. Finotello F, Mayer C, Plattner C, et al. Molecular and pharmacological modulators of the tumor immune contexture revealed by deconvolution of RNA-seq data. *Genome Medicine*. 2019;11(1):34.
4. Stuart T, Butler A, Hoffman P, et al. Comprehensive Integration of Single-Cell Data. *Cell*. 2019;177(7):1888-1902.e21.
5. Oliveira G, Stromhaug K, Klaeger S, et al. Phenotype, specificity and avidity of antitumour CD8+ T cells in melanoma. *Nature*. 2021;596(7870):119–125.
6. Penter L, Gohil SH, Huang T, et al. Coevolving JAK2V617F+ relapsed AML and donor T cells with PD-1 blockade after stem cell transplantation: an index case. *Blood Adv*. 2021;5(22):4701–4709.
7. Heaton H, Talman AM, Knights A, et al. Souporcell: robust clustering of single-cell RNA-seq data by genotype without reference genotypes. *Nat Methods*. 2020;17(6):615–620.
8. Efremova M, Vento-Tormo M, Teichmann SA, Vento-Tormo R. CellPhoneDB: inferring cell–cell communication from combined expression of multi-subunit ligand–receptor complexes. *Nat Protoc*. 2020;15(4):1484–1506.
9. Bachireddy P, Azizi E, Burdziak C, et al. Mapping the evolution of T cell states during response and resistance to adoptive cellular therapy. *Cell Reports*. 2021;37(6):109992.
10. Penter L, Zhang Y, Savell A, et al. Molecular and cellular features of CTLA-4 blockade for relapsed myeloid malignancies after transplantation. *Blood*. 2021;137(23):3212–3217.
11. van Galen P, Hovestadt V, Wadsworth Ii MH, et al. Single-Cell RNA-Seq Reveals AML Hierarchies Relevant to Disease Progression and Immunity. *Cell*. 2019;176(6):1265-1281.e24.
12. Hay SB, Ferchen K, Chetal K, Grimes HL, Salomonis N. The Human Cell Atlas bone marrow single-cell interactive web portal. *Experimental Hematology*. 2018;68:51–61.
13. Wu TD, Madireddi S, de Almeida PE, et al. Peripheral T cell expansion predicts tumour infiltration and clinical response. *Nature*. 2020;579(7798):274–278.
14. Yost KE, Satpathy AT, Wells DK, et al. Clonal replacement of tumor-specific T cells following PD-1 blockade. *Nature Medicine*. 2019;25(8):1251–1259.
15. Oh DY, Kwek SS, Raju SS, et al. Intratumoral CD4+ T Cells Mediate Anti-tumor Cytotoxicity in Human Bladder Cancer. *Cell*. 2020;181(7):1612-1625.e13.
16. Oliveira G, Stromhaug K, Cieri N, et al. Landscape of helper and regulatory antitumour CD4+ T cells in melanoma. *Nature*. 2022;605(7910):532–538.